JOURNAL OF MATERIALS SCIENCE **39** (2004) 3413–3423

Water vapor transport in liquid crystalline and non-liquid crystalline epoxies

JIANXUN FENG*
Department of Materials Science & Engineering, University of Florida, Gainesville, Florida 32611, USA

K. R. BERGER
Agricultural & Biological Engineering Department, University of Florida, Gainesville, Florida 32611, USA

E. P. DOUGLAS‡
Department of Materials Science & Engineering, University of Florida, Gainesville, Florida 32611, USA
E-mail: edoug@mse.ufl.edu

This paper presents a comparison of moisture permeation in liquid crystalline and non-liquid crystalline epoxy systems. The permeability is obtained using a dynamic method. It is found that diffusion in both epoxy systems is Fickian. The liquid crystalline epoxy network exhibits higher barrier properties to moisture transport than the conventional epoxy network. The efficient chain packing of the smectic mesophase of the liquid crystalline epoxy is the main factor for this difference. The stoichiometry has a large effect on the moisture permeation. The diffusion coefficient decreases monotonically with increasing amine/epoxide functional ratio. The permeability (*P*) and solubility coefficient (*S*) reach a minimum for a functional ratio of one. The results are described on the basis of hydrogen bonding of water to the epoxy network and the two phase morphology of cured epoxies. © *2004 Kluwer Academic Publishers*

1. Introduction

Liquid crystalline thermosets (LCT's) are a class of material that combines the advantages of both liquid crystalline polymers and conventional thermosets. For structural applications, an important consideration is the impact of the service environment on the mechanical properties. Moisture affects the properties of epoxies by plasticization, creation of internal stresses, and/or induction of crack growth in the resin [1–5].

A number of structural features clearly can influence the sorption and transport of moisture in epoxies. Water may form hydrogen bonds with the amine and hydroxyl groups present in amine-cured epoxies, effectively slowing the diffusion process. In general, the diffusion coefficient can be expressed as:

$$D = \frac{1}{6} f \times d^2 \tag{1}$$

where f is the jump frequency and d is the jump distance. Hydrogen bonding reduces the jump frequency, while the concentration of hydrogen bonding sites affects the jump distance. Another important factor is the presence of free volume, which provides the pathway for diffusion. Finally, one must consider the heterogeneous nature of cured epoxies. It is well-known that amorphous epoxies exhibit two phases after curing. Most of the evidence comes from electron microscopy conducted on replicas of free and fracture surfaces [6–9], but the two phase structure has also been observed by small angle X-ray scattering [10], dark field transmission electron microscopy [11], and more recently AFM [12]. This two phase structure consists of a hard phase of high crosslink density in a matrix of low crosslink density. This structure has been proposed to occur via initial formation of microgels, which deplete their immediate neighborhood of reactants. At the later stages of cure the regions between the microgel particles crosslink to form the soft phase [12, 13]. It is expected that this two phase structure will have a significant influence on the properties, and qualitative correlations have been described between the mechanical properties or diffusion coefficient and the amount of hard phase present [12, 14, 15].

Studies on the sorption and transport of water in epoxies generally follow two approaches. On the one hand, some researchers emphasize the role of hydrogen-bonding between water and the epoxy network [16–21].

* *Current address*: Den-Mat Corporation, Santa Maria, CA, USA.
‡ Author to whom all correspondence should be addressed.

For others, the structure of the epoxy is considered to be the primary factor governing sorption and transport [15, 22, 23]. In only a few cases are the two effects considered together. Adamson identified three distinct stages of water sorption, and postulated that those stages correspond to water first entering the free volume, then water becoming bound to hydrogen-bonding sites, and finally water entering the more densely crosslinked phase [24]. In a series of papers, Soles *et al*. carefully examined the role of free volume or "nanopores," concluding that transport is primarily governed by the hydrogen bonding of water to the epoxy [25–27]. However, they did not consider the two phase structure of epoxies in their analysis.

The dual-sorption model has been shown to be effective in describing the diffusion of gases in a variety of polymers [28–38]. This model was developed to explain the apparent concentration dependence of the diffusion coefficient. It postulates that gases diffusing in polymers are present in two distinct populations. The first population is that of molecules which are dissolved in the polymer, and is described by Henry's Law. The second population is termed Langmuir sorption, and corresponds to those molecules that are sorbed within voids or holes. The molecules that exhibit Langmuir sorption are assumed to be partially or fully immobilized at these sites, which lowers the effective diffusion coefficient. The concentration dependence of the measured diffusion coefficient arises due to changes in the relative amounts of molecules that occupy each of these two populations. The dual sorption concept has been used to describe the sorption of moisture in epoxies. Barrie *et al*. used the original concept of Langmuir sorption as being caused by voids [39], while Apicella *et al*. explicitly described the Langmuir sorption as being caused by the hydrogen bonding of water molecules to the epoxy [40]. Barrie *et al*. have pointed out that these two concepts are not mutually exclusive, as the accessible hydrogen bonding sites are likely to exist at the surface of these voids [39]. This point is further emphasized in the discussion of moisture transport by Soles *et al.* [25–27].

For heterogeneous polymer systems, the role of two phases with differing permeabilities or diffusion coefficients must also be considered. Various approaches have been taken for systems ranging from semicrystalline polyethylene to liquid crystalline polymers [41–45]. The common feature among all these approaches is that one phase is considered impermeable, and thus diffusion only occurs through the second phase. The reduction in the observed permeability as a result of the impermeable phase is caused by a reduced volume of material available to the permeant and an increased tortuosity for the path the permeant must take through the material. The formalism for describing permeability in these cases ranges from simply reducing the diffusion coefficient and permeability by the fraction of impermeable phase [41], to reducing the diffusion coefficient by a "geometric impedance factor," [42] to a more complex resistance model [44]. In one case an analytical model for moisture diffusion in epoxies explicitly accounts for the heterogeneous morphology, although in that case the hard phase was arbitrarily identified as being hydrophilic and the soft phase as being hydrophobic [23]. Vanlandingham *et al*. have discussed qualitatively how changes in the heterogeneous morphology with amine/epoxide stoichiometry affect the transport process [15].

While there has been extensive work describing moisture sorption for conventional epoxies, there is only limited information available regarding diffusion in liquid crystalline epoxies [46, 47]. Many questions remain to be answered, such as the difference in moisture permeability between liquid crystalline and conventional epoxy thermosets, the mechanism of water sorption and transport, and how the diffusion coefficient, permeability and solubility coefficient change with processing parameters. The aim of this study is to answer the above questions by comparing liquid crystalline and non-liquid crystalline epoxies, and relating the measured diffusion properties to both the hydrogen bonding between water and the epoxy, and the microstructure of the materials.

2. Experimental

2.1. Materials

The isotropic epoxy DER383 was supplied by The Dow Chemical Company. Diglycidyloxy-α-methylstilbene (DOMS) was synthesized as described in the literature [47]. Sulfanilamide (SAA) was purchased from Aldrich Chemical Company and used as received. The epoxide equivalent weight (EEW) of DOMS was determined using standard techniques [48]. The EEW of DER383 was reported by Dow to be 176-183; an average value of 180 was used in all calculations. The chemical structures of the materials are shown in Fig. 1.

Molds for casting samples consisted of a pair of aluminum plates which were sanded with silicon carbide sandpaper, polished, cleaned with water and acetone, sprayed with nonstick release agent (Crown® 6075) purchased from Fisher Scientific, baked at 200°C for 2 h, then cleaned to sweep out the extra Teflon powder. In order to prepare samples for testing, DOMS or DER383 was first melted at 150°C in a convection oven.

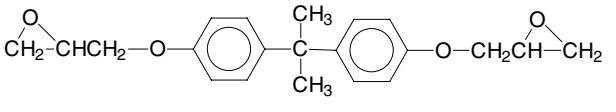

DER383

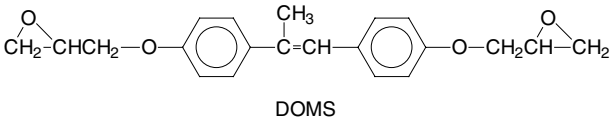

DOMS

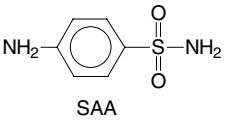

SAA

Figure 1 Chemical structures of DER383, DOMS and SAA.

SAA was then added to the resin. This mixture was periodically stirred over the next 15 min to dissolve all the SAA into the resin. Once all the SAA had dissolved, the mixture was degassed and then poured onto a preheated aluminum plate (dimension = 300 mm × 300 mm × 15 mm) with a Teflon spacer (thickness = 0.1 mm). After about 10 min, a second aluminum plate was put on the top of the first one. Samples were cured for 4 h at 150°C, then the temperature raised at 2°C/min to 175°C, held for 1 h, then raised at 2°C/min to 200°C, and held for 4 h.

After curing, an opaque, cream colored film was obtained for DOMS-SAA samples. The DER-SAA samples were transparent. Specimens were removed from the mold. Tested film samples were cut into the shape of a circle. The radius was about 30 mm, and the thickness 100 μm. To ensure measurement precision, only samples with a thickness variation of less than ± 5 μm were used. The samples were masked with aluminum foil around the edges on both sides and temporarily placed in a vacuum desiccator until further measurement.

Samples are designated as either DOMS-SAA-*X* or DER-SAA-*X* to indicate which monomer is used, where *X* is the ratio of amine reactive sites to epoxy reactive sites.

2.2. Atomic force microscopy

Atomic force microscopy (AFM) was performed using a Digital Instruments Nanoscope III. Measurements were done in Tapping Mode® using a silicon tip with a 125 μm cantilever. Scans were performed over a 1 μm × 1 μm area at a scan rate of 1–2 Hz. The setpoint was adjusted for each sample to obtain the highest quality image, and ranged from 47 to 93% of the free oscillation amplitude, but was typically approximately 50%. This range of setpoints corresponds to hard tapping, which emphasizes the phase image. Both amplitude and phase were recorded in order to obtain topographic and phase images, respectively.

2.3. Density

In order to minimize the effect of sorption on the density measurement, samples were thicker, approximately 25 × 20 × 1.5 mm. Measurement of density is based on the Archimedes principle. An electric analytic digital balance Mettler Toledo AT201 and Density Kit was used. The dry weight of the sample was measured first. The sample was then suspended from the balance and immersed in distilled water to measure the weight of the sample in water. This allowed the density of the sample to be calculated. The moisture uptake during the experiment was negligible, which was confirmed by weighing the dry sample before and after immersing in water.

2.4. Infrared spectroscopy

FTIR analysis was done on a Magna-IR E.S.P. System 760 spectrometer with Nicolet's OMNIC software. DTGS KBr was selected as the detector. The cured epoxy film was mounted in the sample holder. Absorbance spectra at 4 cm^{-1} resolution were obtained using 256 sample and reference scans. In order to ensure that Beer's law applies for quantitative analysis, the sample thicknesses were such that the maximum absorbance of any spectral feature was less than 1.0.

After collecting the spectra of the dry samples, the samples were soaked in deionized water and allowed to equilibrate. The soaking time was estimated according to the diffusion coefficient and the samples were given extra time to ensure equilibrium had been reached. At room temperature, more than 120 min was allowed for the epoxy film to equilibrate in the liquid water environment. Then the samples were placed into the FTIR to collect the spectra of the wet samples. No base-line correction was performed on the spectra. To isolate the effects of moisture on the spectra, spectra of dry samples were subtracted from spectra of wet samples to obtain hydration spectra. For all hydration spectra, the same sample was used for obtaining both the dry spectrum and the wet spectrum. It was assumed that there are no changes in the sample thickness upon moisture absorption, and thus no normalization of the spectra was performed. Quantitative analysis was performed by deconvoluting the spectra over the range of 3700 to 3100 cm^{-1} with three Lorentzian peaks; details of the peak assignments are given in the Results and Discussion section.

2.5. Permeability

A MOCON Permatran-W3/31 Water Vapor Permeation Measurement System with an IR detector was used to measure and analyze the water vapor transmission rate. The test film was first placed into the test cell, and then flushed with dry nitrogen gas on both sides to degas moisture absorbed during sample installation. HPLC-grade water was then introduced into sponges, located in the outer cover of the test cell, by injection through the hole on the outside of the cell. As the water vapor diffused through the test film, it was carried by nitrogen carrier gas to the detector, and the water vapor transmission rate (WVTR) was continuously recorded. The nitrogen gas flow was set at 10 sccm (standard cubic centimeters per minute). To ensure system accuracy in determining water vapor transmission rates and to compensate for environmental variations that affect the system, such as room temperature, a calibration procedure was performed to compensate for these variables. A certified reference film (WVTR = 0.00120 g/package/day, 40.38 cm^2, 10 sccm, 37.8°C, 100%RH) was used for the calibration. This film was obtained from Modern Controls Inc. The reference film was individually tested with test equipment traceable to NIST.

3. Results and discussion

3.1. Atomic force microscopy

In this study, AFM was performed in Tapping Mode® in order to image the two phase structure. A typical image is shown in Fig. 2, in which the hard domains are the light regions. In this image, the contrast is due to

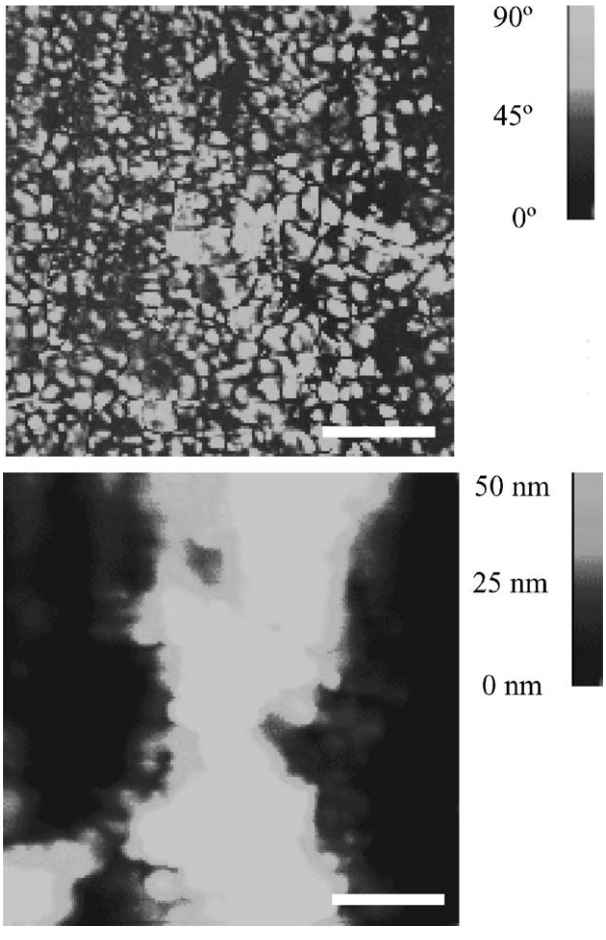

Figure 2 Phase (upper) and topographic (lower) AFM images of DER-SAA-0.9. In the phase image, light regions represent the hard phase and dark regions represent the soft phase. Scale bar represents 0.25 μm.

the phase lag induced by interaction of the oscillating tip with the sample. Many factors, such as viscoelasticity of the sample and adhesion between the tip and the sample may affect the phase image, and in fact contrast may be reversed in a single sample by simply adjusting the acquisition parameters [49]. Our assignment of the light regions in the image to the hard phase is based on density measurements, described below. Another factor that may affect the phase image is topography. In order to check this, the topographic images were also examined, and an example is also shown in Fig. 2 for the same region as the phase image. Although there is some topographic variation, it is on a larger scale than the structures seen in the phase image, and there is no correlation between the topographic and phase images. Thus we can conclude that the phase images reflect the properties of the material.

In order to calculate the volume fractions of the hard and soft phase present and to determine which regions of the images correspond to the hard and soft phases, images such as Fig. 2 were analyzed as to the relative amounts of bright (phase angles of 70°–90°) regions and dark (phase angles of 0°–45°) regions present and compared to the density measurements. For each sample, AFM images were obtained from three different regions and the results averaged. The results are shown in Figs 3 and 4. We note that the shapes of the curves in each of these figures is the same. This is expected, since the higher crosslink density phase is expected to have a higher density, resulting in an overall higher density for samples with a higher fraction of that hard phase. Therefore, we can conclude that the light regions on the image correspond to the hard phase. Overall, the stoichiometric ratio has a higher percentage of hard phase than nonstoichiometric ratios, although the difference is barely significant given the error bars of Fig. 3. We would expect that non-stoichiometric ratios would have a lower fraction of hard phase, because those compositions will have unreacted end-groups (either amine or epoxy) that can not contribute to crosslinking.

Overall, our results similar to those obtained by Vanlandingham *et al.* on a different epoxy system [12], indicating that the phase structure in epoxies as observed by AFM is a general phenomenon. Our main aim here is to provide a partial explanation for the observed permeability behavior, to be described later.

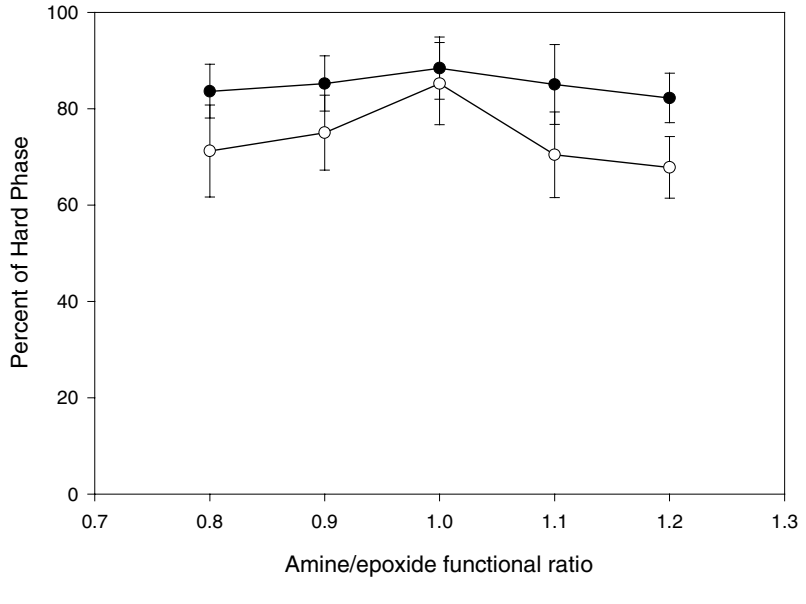

Figure 3 Percentage of hard-phase for DER-SAA and DOMS-SAA. (●): DER-SAA; (○): DOMS-SAA.

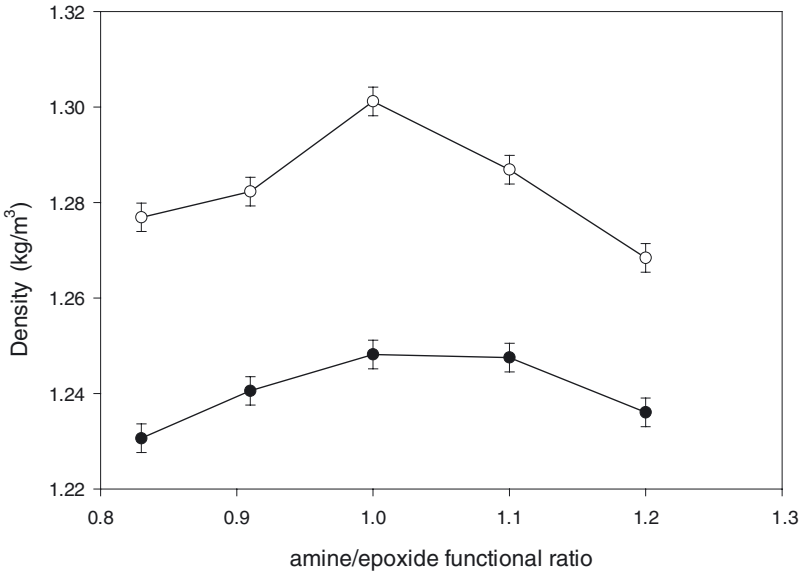

Figure 4 Density of DER-SAA and DOMS-SAA. (●): DER-SAA; (○): DOMS-SAA.

3.2. Infrared spectroscopy

A large number of studies have examined the bonding of water in epoxies, aiming to identify the precise nature of the bonding as well as the property changes that result [16–21]. It is clear that there are a number of sites available in the cured epoxy at which water may form hydrogen bonds. In addition, some water is considered to be "free water," that is water molecules that are not hydrogen-bonded. As with the AFM, our primary aim here is to provide some experimental data to explain the observed permeability.

Fig. 5 shows the full FTIR spectrum of a dry epoxy sample, the same sample fully hydrated, and the difference spectrum. This difference spectrum reflects the spectrum of water in the epoxy. The region from 3700 to 3100 cm^{-1} was deconvoluted into three peaks, and the results are shown in Fig. 6. The band at high wavenumbers is assigned to free water, the middle band is assigned to water hydrogen-bonded to hydroxyl groups, and the band at low wavenumbers is assigned to water hydrogen-bonded to amine groups. We should note that we also attempted to fit this region of the spectrum with two, four, or five bands, but these attempts yielded poor fits and the positions of these bands have no physical meaning. These assignments are consistent with previous assignments [50, 51]. In particular we note that previous work has found that the water sorption process is reversible, indicating that the water does not react with free epoxy groups [50, 52], and that the hydrogen bond network present in dry samples is not disrupted by the sorbed water [51].

Quantitative analysis of hydrogen bonding with FTIR spectra is based upon Beer's law. Often it is assumed that the absorption coefficient is the same for the

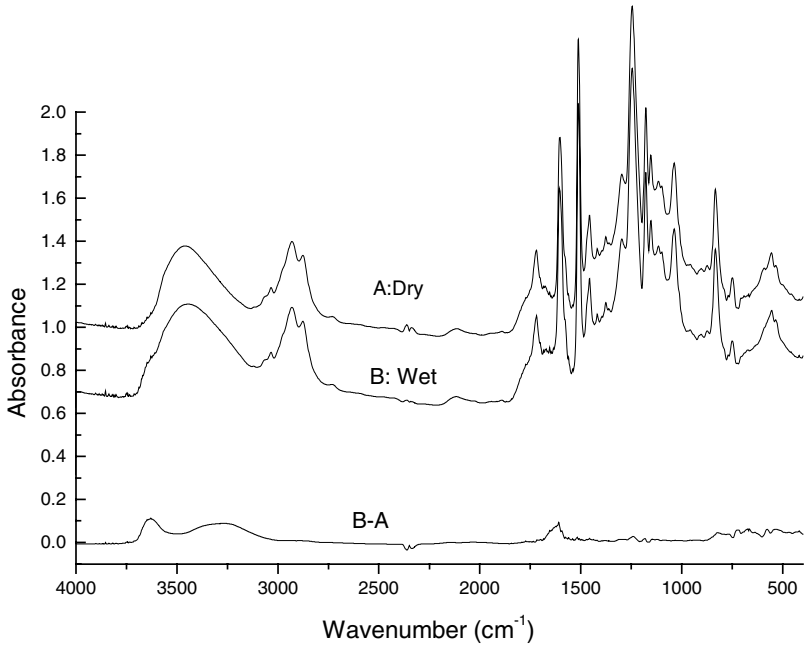

Figure 5 Spectra of cured DOMS-SAA-0.8 samples.

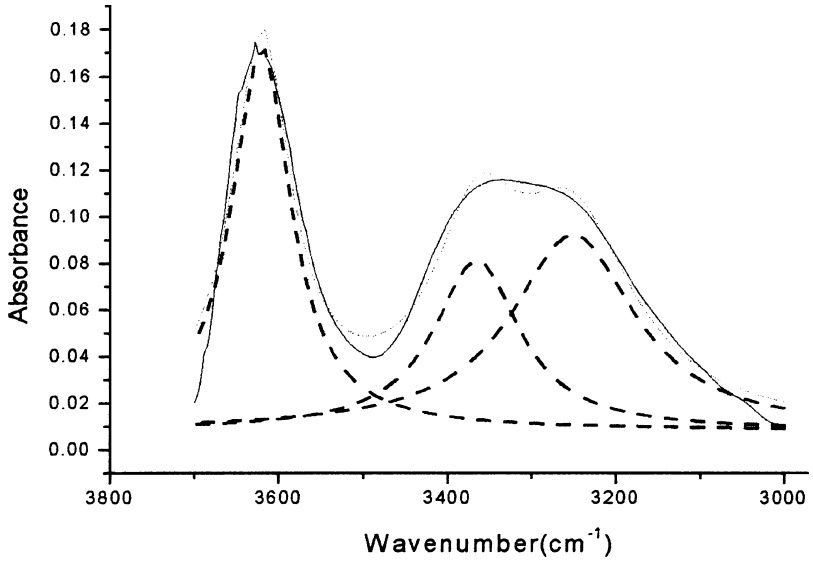

Figure 6 Curve fitting for DOMS-SAA-0.8 sample. Solid line: experimental data; dashed lines: fitted peaks; dotted line: sum of the fitted peaks.

hydrogen-bonded and non-hydrogen-bonded species, allowing the relative peak areas to be used for quantitative analysis. However, it has been pointed out that for the O─H stretch region under consideration here, the absorption coefficient can exhibit a strong dependence on wavenumber [51]. Since we do not know the absorption coefficients for the different species under consideration, the quantitative analysis below is based on the relative peak areas only. Even though the absolute concentrations or fractions of the different species can not be calculated, we can still discuss relative trends, since the relative peak areas differ from the concentrations by a constant factor. Thus, although we discuss the FTIR data in terms of the fractions of species present, it should be kept in mind that these data are actually the ratios of peak areas, which differ from the fraction present by an unknown constant.

Fig. 7 shows the change in the relative fractions of hydrogen-bonded and free water as a function of the stoichiometry. For both DER-SAA and DOMS-SAA, the percentage of hydrogen-bonded water increases with increasing stoichiometric ratio. This is not unexpected. As the amount of SAA increases in the cured resin, the amount of polar groups increases because the concentration of hydroxyl groups and/or amine groups increases. These polar groups tend to interact with water molecules to form hydrogen bonds. We also note that there is more hydrogen-bonded water in the liquid crystalline material. Although this may seem counterintuitive, it can be explained by considering that the band for water hydrogen-bonded to hydroxyl groups includes the contributions from water bonded to hydroxyl groups in the epoxy network and water bound to itself. In the case of DER-SAA, it is relatively easier for water to diffuse into the high density regions, where it exists as either free water or water bound to the polar groups. For DOMS-SAA, however, there is less water present in these high density regions due to

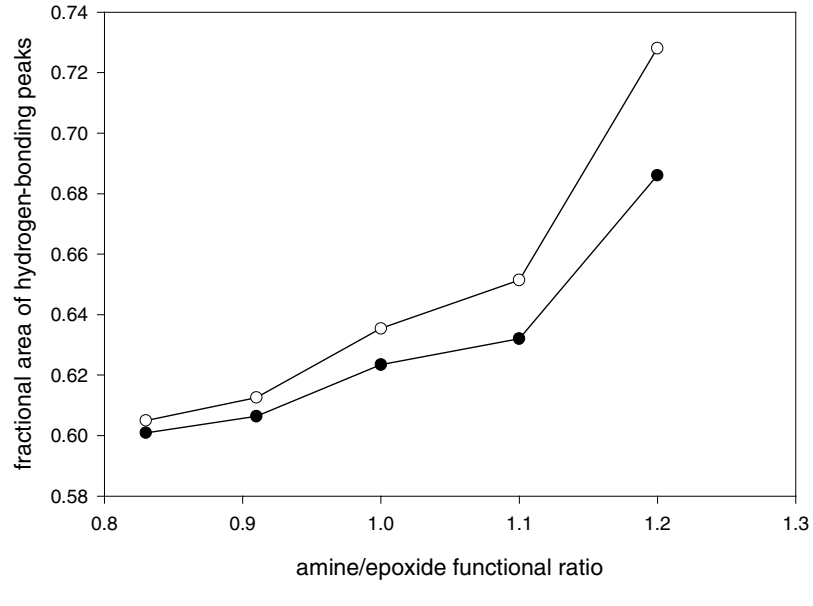

Figure 7 Fractional area of peaks corresponding to hydrogen-bonded water compared to total area of peaks associated with water in saturated samples. (●): DER-SAA; (○): DOMS-SAA.

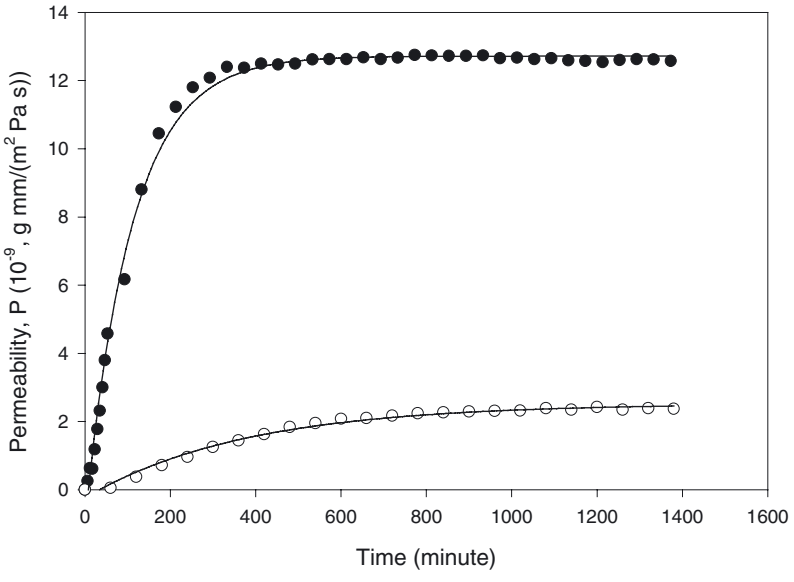

Figure 8 Typical water vapor permeation rate curves measured at 37.8°C. (●): DER-SAA-1.0; (○): DOMS-SAA-1.0. Solid lines are fits to the data for Fickian diffusion.

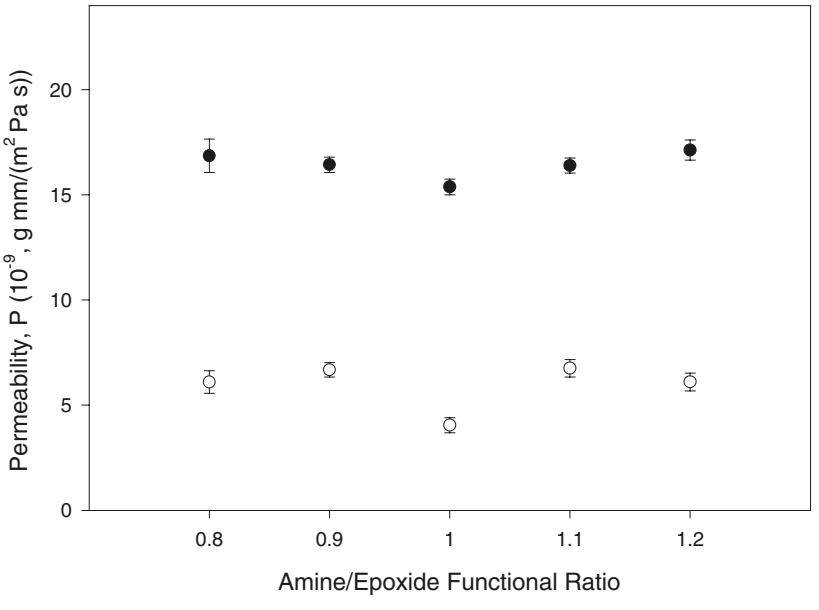

Figure 9 Relationship between permeability and amine/epoxide functional ratio at 30°C. (●): DER-SAA; (○): DOMS-SAA.

the additional barrier of the smectic mesophase, and thus more water is in the low density regions where it is hydrogen bonded to itself in clusters. Thus, the overall percentage of hydrogen-bonded water is greater for DOMS-SAA than for DER-SAA.

3.3. Permeability

Permeability was obtained by measuring the total transport through the epoxies as a function of time. Fig. 8 shows typical data for this measurement. The line in this figure is a fit of the data based on Fickian diffusion. In all cases the diffusion is Fickian. Non-Fickian diffusion in polymers is generally described as being caused by relaxation of the chains induced by the penetrant [15, 53, 54]. Both DOMS and DER are highly crosslinked materials, and the rigid nature of the network would thus not be expected to undergo the types of changes leading to non-Fickian diffusion.

Permeability was determined from the steady-state water vapor transmission rate through the film according to:

$$P = \frac{WVTR \times L}{VP \times (R_1 - R_2)} \tag{2}$$

where L is the film thickness, VP is the vapor pressure of water at the test temperature, R_1 is the relative humidity at the source, expressed as a fraction, and R_2 is the relative humidity on the far side of the film. For our measurements, $R_1 = 1$ and $R_2 = 0$. The diffusion coefficient was determined from the half-time:

$$D = \frac{\ln 4}{\pi^2} \frac{L^2}{t_{1/2}} \tag{3}$$

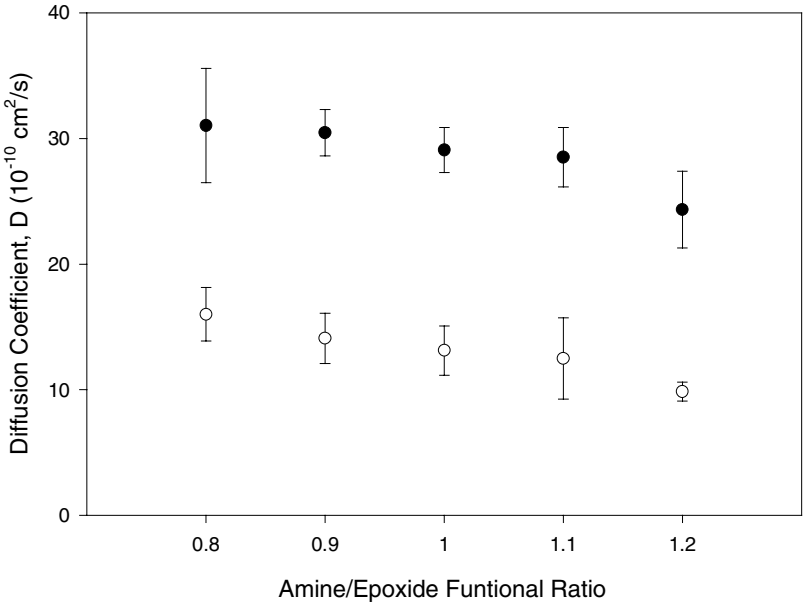

Figure 10 Relationship between diffusion coefficient and amine/epoxide functional ratio at 30°C. (●): DER-SAA; (○): DOMS-SAA.

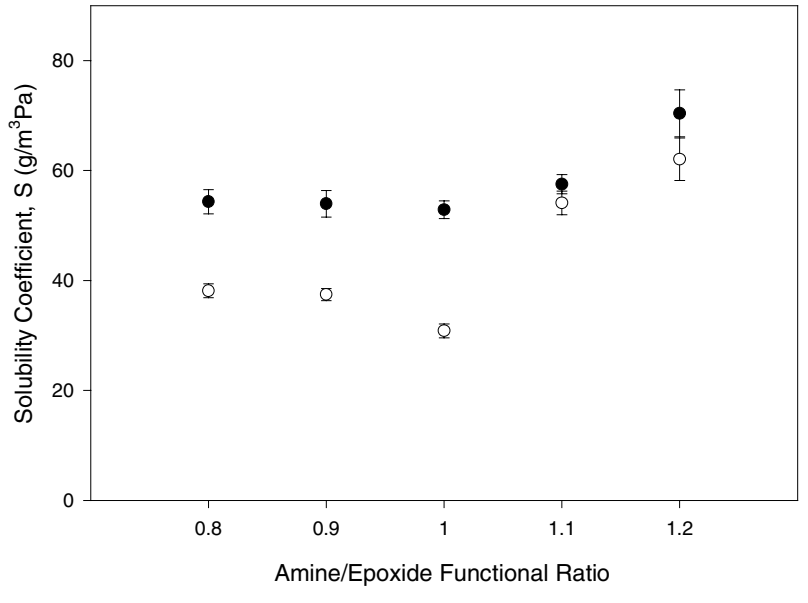

Figure 11 Relationship between solubility coefficient and amine/epoxide functional ratio at 30°C. (●): DER-SAA; (○): DOMS-SAA.

where $t_{1/2}$ is half the time required to reach steady-state. Once the diffusion coefficient and the permeability are known, the solubility can be determined from:

$$S = \frac{P}{D} \tag{4}$$

Figs 9–11 show the effects of stoichiometry and liquid crystallinity on permeability, diffusion coefficient and solubility. It is obvious that the diffusion coefficient and permeability of DOMS-SAA are much lower than that of DER-SAA. This difference can be attributed to the liquid crystalline structure of DOMS-SAA [55–57]. It has previously been shown that liquid crystalline polymers exhibit higher barriers to diffusion [43–45, 58], and thus it is perhaps not surprising that the same behavior is observed in liquid crystalline thermosets. Our results are similar to Earls *et al*. who found a difference in sorption between DOMS-SAA and DER-SAA for various solvents [47]. However, Carfagna *et al*. found that there is no difference in moisture sorption for DOMS when it is cured in the nematic or isotropic state [46]. The difference between our results and those of Carfagna is that in our case the liquid crystalline phase present is smectic, leading to a higher barrier compared to the nematic or isotropic phase.

For the diffusion coefficient, D, a monotonic decrease with increasing amine/epoxide functional ratio at different test temperatures is seen for all samples. This is the same behavior observed previously [15]. Both the solubility coefficient and the permeability reach a minimum at stoichiometric ratio for all temperatures studied. The effect of stoichiometry on moisture diffusion can be explained by the above two factors of morphological heterogeneity and hydrogen bonding site concentration.

The trend of D with stoichiometric ratio can be attributed to the presence of two phases and to the

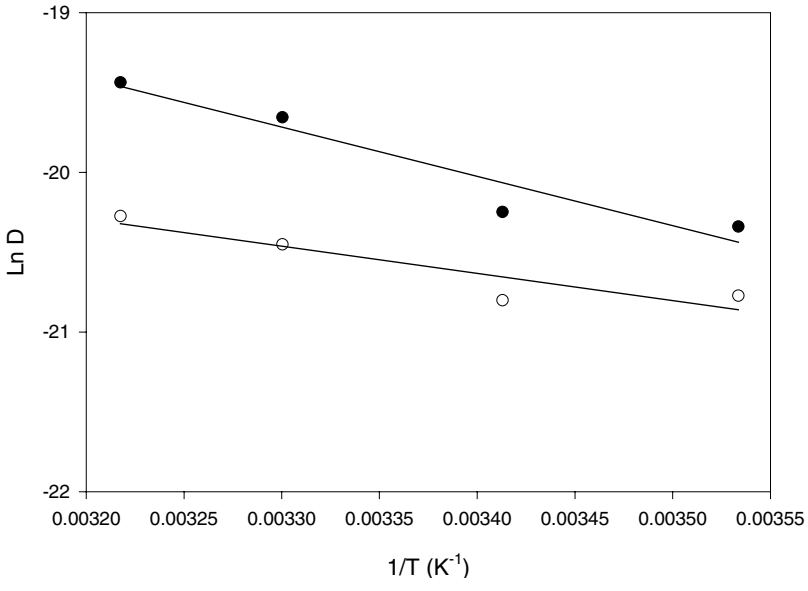

Figure 12 Arrhenius plot of diffusion coefficients. (●): DER-SAA-1.0; (○): DOMS-SAA-1.0.

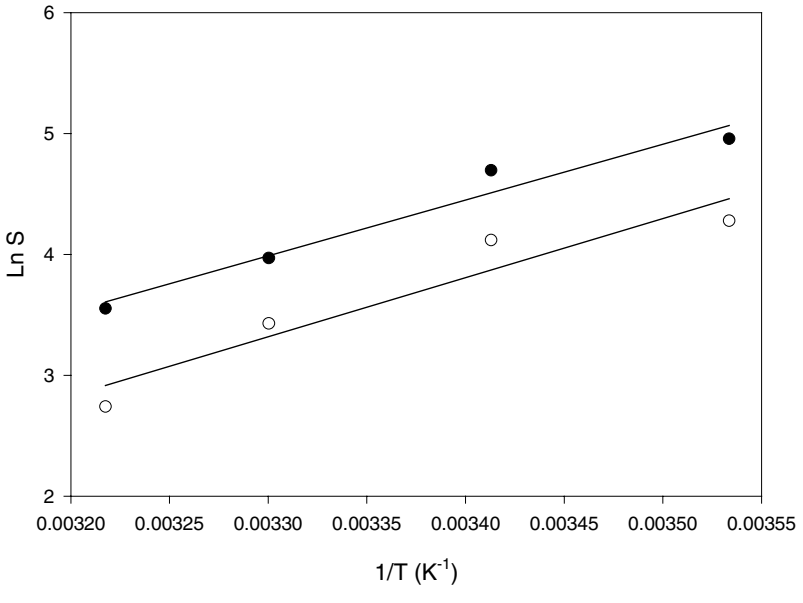

Figure 13 Van't Hoff plot of solubility coefficients. (●): DER-SAA-1.0; (○): DOMS-SAA-1.0.

hydrogen bonding interaction between water and polar groups in the cured resin. For epoxy-rich samples, the fraction of hard phase increases slightly with increasing functional ratio. The hard phase acts as a blockade against the diffusing water molecules, effectively slowing their advance. Therefore, the diffusion coefficient decreases with increasing percentage of hard phase. For amine-rich samples, however, the fraction of hard phase decreases with increasing functional ratio. Surprisingly, the diffusion coefficient decreases with the amine/epoxide functional ratio. This is an unexpected result. If the two-phase morphology played a major role in determining D, it would be expected that D would increase with SAA concentration. The experimental result can be attributed to the increasing number of polar groups as the amine/epoxide ratio increases. Water molecules are fixed to polar sites in the network through hydrogen bonding. As the amine/epoxide functional ratio increases, more of these polar groups exist, and a greater amount of the absorbed water is bonded at these sites. The water molecules are effectively bound at these sites. The result is that the diffusion process is slowed down, and the diffusion coefficient will, therefore, decrease with increasing amine/epoxide functional ratio. This description is consistent with that of Soles *et al*., which emphasizes the role of hydrogen bonding in controlling transport behavior [26].

In a similar fashion, the trend of S with stoichiometric ratio can also be attributed to the presence of two phases and to the hydrogen bonding interaction between water and polar groups in the cured resin. For epoxy-rich samples, the primary factor in determining the solubility is the two-phase morphology. It is reasonable to assume that the absorbed water prefers to occupy the low crosslink density phase because the free volume is higher in that region. Again, the fraction of this phase decreases with the amine/epoxide functional ratio, and therefore the amount of sorbed water should decrease with increasing stoichiometric ratio. Since for epoxy-rich samples the amine concentration

is low, hydrogen bonding to these groups plays only a minor role in determining the overall solubility. For amine-rich samples, both the two-phase morphology and the change in polar group concentration contribute to the change in solubility with stoichiometry. First, increasing the amine/epoxide functional ratio increases the percentage of soft phase and free volume. Thus, there is more space for water molecules to occupy in the cured resin and the solubility increases with stoichiometric ratio. Simultaneously, the concentration of polar groups increases. Therefore, not only can penetrating water molecules occupy the greater amount of free volume present, they can also bind at the additional polar sites. This allows more water molecules to absorb into the resin, and S increases with functional ratio for the amine rich networks. Soles *et al*. also showed that the isothermal equilibrium weight gains are a function of the free volume fraction and polarity for rigid, semi-rigid and flexible epoxy networks [25].

The effect of temperature on diffusion coefficient and solubility are shown in Figs 12 and 13. The diffusion coefficient follows the Arrhenius relation. Table I provides the activation energies. At first glance it is somewhat surprising that DOMS-SAA has a lower activation energy than DER-SAA. However, we can explain this phenomenon using the same argument used by Vanlandingham *et al*. to explain the varying activation energies for isotropic epoxies of different stoichiometries. The activation energy describes the temperature dependence of the diffusion coefficient. DOMS is a more rigid molecule than DER, and thus we would expect that temperature would have a smaller effect on molecular mobility for DOMS than for DER. The weaker dependence of mobility on temperature would thus translate into a lower activation energy for diffusion, since temperature will have a weaker effect on the diffusion coefficient for the less mobile material. The solubility is found to follow a van't Hoff relation, and the heats of solution are shown in Table I. The heats of solution become more negative with increasing amine content. Since the formation of hydrogen bonds is an exothermic process, the results suggest that there is more hydrogen bonding with increasing amine content, consistent with the FTIR results.

Finally, we note that the trends in diffusion coefficient, solubility, and permeability are identical for DOMS-SAA and DER-SAA. This suggests that the same mechanism is operating in both materials, and the discussion above is independent of the presence or absence of the liquid crystalline phase. Thus, the role of the liquid crystalline phase is simply to provide a barrier to slow the diffusion process, but does not affect the fundamental nature of how that diffusion occurs.

TABLE I Activity energy of diffusion and heat of solution

System	Amine/epoxide functional ratio	Activity energy of diffusion (kJ/mol)	Heat of solution (kJ/mol)
DER-SAA	0.8	21.7	−36.2
	0.9	22.5	−38.4
	1.0	25.7	−39.5
	1.1	21.0	−40.0
	1.2	20.0	−42.8
DOMS-SAA	0.8	10.9	−31.8
	0.9	11.5	−35.7
	1.0	14.2	−40.6
	1.1	14.1	−41.0
	1.2	13.2	−41.7

4. Conclusions

The moisture permeation process for both the conventional epoxy system and the liquid crystalline epoxy system follows Fick's law. The high cross-linking density is responsible for this behavior. The liquid crystalline epoxy network exhibits higher barrier properties to moisture permeation than the conventional epoxy network. The efficient chain packing of the smectic mesophase of the liquid crystalline thermoset (LCT) is the main factor for this difference. The close packing of molecules in the liquid crystalline phase causes a reduction in free volume compared to the isotropic epoxy. Thus, the liquid crystalline domains act as barriers for the diffusion of the permeant through the matrix.

The curing conditions, such as the stoichiometry, have a strong effect on the moisture permeation properties. The diffusion coefficient decreases monotonically with increasing amine/epoxide functional ratio. The permeability (P) and solubility coefficients (S) reach a minimum when the functional ratio equals one. The influence of the stoichiometry on D, P, and S can be explained on the basis of the two-phase morphology of epoxies and hydrogen bonding interaction between absorbed water and the network. These factors are the same for both the liquid crystalline and isotropic systems, and thus the mechanism of diffusion is the same in these two materials.

Acknowledgments

This work was supported by the U.S. Army Research Office under Grant DAAG55-98-1-0114 to Dr. Elliot P. Douglas as a Presidential Early Career Award for Scientists and Engineers.

References

1. M. G. LU, M. J. SHIM and S. W. KIM, *J. Appl. Polym. Sci.* **81** (2001) 2253.
2. G. Z. XIAO and M. E. R. SHANAHAN, *ibid.* **69** (1998) 363.
3. G. Z. XIAO, M. DELAMAR and M. E. R. SHANAHAN, *ibid.* **65** (1997) 449.
4. B. DENEVE and M. E. R. SHANAHAN, *Polymer* **34** (1993) 5099.
5. R. L. LEVY, D. L. FANTER and C. J. SUMMERS, *J. Appl. Polym. Sci.* **24** (1979) 1643.
6. E. H. ERATH and R. A. SPURR, *J. Polym. Sci.* **XXXV** (1959) 391.
7. E. H. ERATH, *J. Polym. Sci. Pt.* C **3** (1963) 65.
8. J. RACICH and J. KOUTSKY, *J. Appl. Polym. Sci.* **20** (1976) 2111.
9. R. J. MORGAN and J. E. O'NEAL, *J. Mater. Sci.* **12** (1977) 1966.
10. R. J. MATYI, D. R. UHLMANN and J. A. KOUTSKY, *J. Polym. Sci. Pt. B-Polym. Phys.* **18** (1980) 1053.
11. A. OBERLIN, J. AYACHE, M. OBERLIN and M. GUIGON, *ibid.* **20** (1982) 579.
12. M. R. VANLANDINGHAM, R. F. EDULJEE and J. W. GILLESPIE, *J. Appl. Polym. Sci.* **71** (1999) 699.

13. R. A. SPURR, E. H. ERATH, H. MYERS and D. C. PEASE, *Ind. Eng. Chem.* **49** (1957) 1839.
14. J. MIJOVIC and J. A. KOUTSKY, *Polymer* **20** (1979) 1095.
15. M. R. VANLANDINGHAM, R. F. EDULJEE and J. W. GILLESPIE, *J. Appl. Polym. Sci.* **71** (1999) 787.
16. V. BELLENGER, V. VERDU and E. MOREL, *J. Mater. Sci.* **24** (1989) 63.
17. L. W. JELINSKI, J. J. DUMAIS, A. L. CHOLLI, T. S. ELLIS and F. E. KARASZ, *Macromolecules* **18** (1985) 1091.
18. J. ZHOU and J. P. LUCAS, *Polymer* **40** (1999) 5513.
19. *Idem.*, *ibid.* **40** (1999) 5505.
20. C. GRAVE, I. MCEWAN and R. A. PETHRICK, *J. Appl. Polym. Sci.* **69** (1998) 2369.
21. Y. F. DING, M. J. LIU, S. J. LI, S. Y. ZHANG, W. F. ZHOU and B. WANG, *Macromol. Chem. Phys.* **202** (2001) 2681.
22. V. B. GUPTA, L. T. DRZAL and M. J. RICH, *J. Appl. Polym. Sci.* **30** (1985) 4467.
23. C. MAGGANA and P. PISSIS, *J. Polym. Sci. Pt. B-Polym. Phys.* **37** (1999) 1165.
24. M. J. ADAMSON, *J. Mater. Sci.* **15** (1980) 1736.
25. C. L. SOLES, F. T. CHANGE, B. A. BOLAN, H. A. HRISTOV, D. W. GIDLEY and A. F. YEE, *J. Polym. Sci. Pt. B-Polym. Phys.* **36** (1998) 3035.
26. C. L. SOLES and A. F. YEE, *ibid.* **38** (2000) 792.
27. C. SOLES, F. T. CHANG, D. W. GIDLEY and A. F. YEE, *ibid.* **38** (2000) 776.
28. W. R. VIETH, J. M. HOWELL and J. H. HSIEH, *J. Membr. Sci.* **1** (1976) 177.
29. E. J. CAIN, W. Y. WEN, A. A. JONES, P. T. INGLEFIELD, B. J. CAULEY and J. T. BENDLER, *J. Polym. Sci. Pt. B-Polym. Phys.* **29** (1991) 1009.
30. T. A. BARBARI, W. J. KOROS and D. R. PAUL, *ibid.* **26** (1988) 709.
31. *Idem.*, *ibid.* **26** (1988) 729.
32. T. C. MERKEL, V. BONDAR, K. NAGAI, B. D. FREEMAN and Y. P. YAMPOLSKII, *Macromolecules* **32** (1999) 8427.
33. V. TEPLYAKOVA, D. ROIZARD, E. FAVRE and V. S. KHOTIMSKY, *J. Membr. Sci.* **220** (2003) 165.
34. T. SUZUKI, H. YOSHIMIZU and Y. TSUJITA, *Polymer* **44** (2003) 2975.
35. B. PEREIRA, W. ADMASSU and J. JENSVOLD, *Sep. Sci. Technol.* **36** (2001) 417.
36. B. PEREIRA and W. ADMASSU, *ibid.* **36** (2001) 177.
37. G. E. SERAD, B. D. FREEMAN, M. E. STEWART and A. J. HILL, *Polymer* **42** (2001) 6929.
38. H. D. KAMARUDDIN and W. J. KOROS, *J. Polym. Sci. Pt. B-Polym. Phys.* **38** (2000) 2254.
39. J. A. BARRIE and P. S. SAGOO, *J. Membr. Sci.* **18** (1984) 197.
40. A. APICELLA, R. TESSIERI and C. D. CATALDIS, *ibid.* **18** (1984) 211.
41. S. W. LASOSKI, JR. and H. W. COBBS, JR., *J. Polym. Sci.* **36** (1959) 21.
42. A. S. MICHEALS and H. J. BIXLER, *ibid.* **50** (1961) 413.
43. D. H. WEINKAUF and D. R. PAUL, *J. Polym. Sci. Pt. B-Polym. Phys.* **29** (1991) 329.
44. *Idem.*, *ibid.* **30** (1992) 817.
45. *Idem.*, *ibid.* **30** (1992) 837.
46. C. CARFAGNA, E. AMENDOLA, M. GIAMBERINO, G. MENSITIERI and M. NOBILE, *Polym. Eng. Sci.* **35** (1995) 137.
47. J. D. EARLS, R. E. HEFNER and P. M. PUCKETT, U.S. Patent no. 5,270,405 Assigned to The Dow Chemical Company, Midland, Mich, USA, 1993.
48. H. JAHN and P. GOETZKY, in "Epoxy Resins: Chemistry and Technology," edited by C. May (Marcel Dekker Inc., New York, 1988).
49. S. N. MAGONOV, V. ELINGS and M. H. WHANGBO, *Surf. Sci.* **375** (1997) L385.
50. V. BELLENGER, J. VERDU, J. FRANCILLETTE, P. HOARAU and E. MOREL, *Polymer* **28** (1987) 1079.
51. P. MUSTO, G. RAGOSTA and L. MASCIA, *Chem. Materr.* **12** (2000) 1331.
52. M. K. ANTOON, J. L. KOENIG and T. SERAFINI, *J. Polym. Sci. Polym. Phys. Ed.* **19** (1981) 1567.
53. T. S. ELLIS and F. E. KARASZ, *Polymer* **25** (1984) 664.
54. E. L. J. MCKAGUE, J. D. REYNOLDs and J. E. HALKIAAS, *J. Appl. Polym. Sci.* **22** (1978) 1643.
55. Q. H. LIN, A. F. YEE, H. J. SUE, J. D. EARLS and R. E. HEFNER, *J. Polym. Sci. Pt. B-Polym. Phys.* **35** (1997) 2363.
56. Q. LIN, A. F. YEE, J. D. EARLS, R. E. HEFNER, JR. and H.-J. SUE, *Polymer* **35** (1994) 2679.
57. B. C. BENICEWICZ, M. E. SMITH, J. D. EARL, J. RAIPH D. PRIESTER, S. M. SETZ, R. S. DURAN and E. P. DOUGLAS, *Macromolecules* **31** (1998) 4730.
58. D. H. WEINKAUF, H. D. KIM and D. R. PAUL, *ibid.* **25** (1992) 788.

Received 19 September 2002
and accepted 5 February 2004